Synthesis of Novel 2-Quinolone linked 1,2,3-Triazole Derivatives as Potent Antimicrobial Activities: *in silico* Docking Studies

Komal Chandrakar, Naveen Kumar Sureddy, S.P. Mahapatra and Santosh Penta[*]

Department of Chemistry, National Institute of Technology, Raipur-492010, India

*Corresponding author: E-mail: spenta.che@nitrr.ac.in

The current research focuses on organic and medicinal chemistry, with a specific emphasis on the synthesis of molecules that incorporate diverse heterocycles. As part of this investigation, we have explored the fusion of 2-quinolone with 1,2,3-triazoles. Analytical and spectral data were applied to elucidate the structure of the synthesized compounds. In the preliminary antibacterial studies, analogs **4a**, **4f**, **6d** and **6a** were more effective against *S. epidermidis* corresponding MIC values of 6.32 ± 0.04, 2.38 ± 0.01, 5.18 ± 0.03 and 14.33 ± 0.01 μg/mL, respectively. In addition, compound **4a** exhibited outstanding antibacterial activity against strains of *Pseudomonas aeruginosa*, as evidenced by a remarkable minimum inhibitory concentration (MIC) value of 3.19 ± 0.04 μg/mL. In particular, the synthesized scaffolds **6d**, **4f**, **4c** and **4a** showed significant antifungal activity with MIC values of 2.70 ± 0.01, 3.74 ± 0.03, 3.16 ± 0.02 and 4.18 ± 0.03 μg/mL against *Candida albicans*. The essential binding mode active site interactions in the DNA gyrase complex from *Staphylococcus aureus* based antibacterial drug candidate with 2XCO protein was also investigated and ligand **4a** possesses the highest interacting amino acid residues ArgA:1092, PheA:1266, LysA:1043, AlaA:1172, AlaA:1034, TyrA:1099, HisA:1046, HisA:1046 [O11···NH], GlnA:1267 [O12···NE2], GlyA:1041 [N14···O, 3.22 Å], ThrA:1181 [O1···N]. The resulting scaffolds were assessed for ADMET and physico-chemical characteristics using ADMETlab2.0server, SwissADME web as good drugs with oral bioavailability.

Keywords: 1,2,3-Triazoles, 2-Quinolones, Antimicrobial activity, Docking techniques, 2XCO, *In silico* studies.

INTRODUCTION

Quinolones, a class of synthetic antibacterial substances, act by inhibiting the production of DNA gyrase and topoisomerase enzymes in bacteria [1]. Since their discovery in the 1970s, Quinolones and their numerous synthetic analogues stand out as highly potent and extensively utilized antibiotics [2]. Functioning by forming ternary enzyme-DNA complexes, quinolones effectively inhibit bacterial RNA transcriptionand DNA repair. Fluoroquinolones, a subtype with broad-spectrum antibiotic activity, find common application in treating various bacterial infections such as chronic prostatitis, shigellosis, cystitis, urinary tract infections and acute sinus problems [3,4]. An essential and versatile method for synthesizing pharmacologically active compounds featuring one or more five-membered heterocycles is the Huisgen 1,3-dipolar cycloaddition reaction (1,3-DCR). This synthesis method meets the stringent requirements set for click chemistry reactions: modularity, good yields,

exclusive production of safe byproducts separable through non-chromatographic methods and stereospecificity without necessarily requiring selective antagonism [5,6].

The application of click chemistry provides prospects for developing new pharmacophores, which display a variety of functional chemical components [7]. The discovery and development of new organic and pharmaceutical chemicals play a pivotal role in advancing various fields and this process is significantly dependent on nitrogen-containing heterocyclic compounds. Triazole derivatives have emerged as significant compounds in the pharmaceutical industry, garnering attention due to their versatile efficacy, well-defined structure, low toxicity and high selectivity. Their utilization aligns with modern green chemistry principles, emphasizing environmentally friendly practices in drug development [8]. In the pursuit of antimicrobial agents, the emphasis is not only on increased effectiveness but also on minimizing toxicity, a crucial consideration in drug discovery and medicinal chemistry. The quinoline and triazole

scaffolds, both incorporating nitrogen-based heterocycles, have proven to be valuable platforms for the synthesis of novel drugs with diverse biological activities [9,10]. Quinolone derivatives, known for their diverse applications, have been employed in the development of innovative therapeutics, such as anti-bacterial, anti-HIV, anti-inflammatory, antifungal, antiplasmo-dial, potential bioactive molecules and anticancer medicines [11,12]. 1,2,3-Triazoles have wide variety of significant bio-logical activities like anti-tuberculosis, anti-inflammatory, anti-microbial, anticonvulsant, antifungal, anticancer, antimalarial, antineoplastic, anti-HIV, herbicidal, potassium channel inhibitors CB1 receptor antagonists [13-23]. This inherent dipole moment enhances the ability of heterocyclic compounds to actively participate in a variety of interactions, such as dipole-dipole interactions, hydrogen bonds and pi-stacking interactions, make them valuable for binding to biomolecular targets [24].

Reviewing the biological properties of quinolone 1,2,3-triazoles, our aim to synthesize new compounds that contain both components and analyze their antifungal and antibacterial activity, because mixing couple of pharmacological agents in a single arrangement is a unique path for making better drugs. Expanding our interest, we synthesized new heterocyclic comp-ounds utilizing various precursors including 2-quinolones with 1,2,3-triazoles. These compounds are highly significant scaff-olds, demonstrating significant antibacterial activity. After our reseAr-Ch analysis as well as with our aim, further molecular docking was performed to study possible interactions with the binding of compounds examined as antibacterial drug against the DNA gyrase complex (2XCO) against *S. aureus* of DNA gyrase complex (2XCO). Additionally, The SwissADMETlab2.0 (https://admetmesh.scbdd.com/)ADME website (http://www.swissadme.ch)was used for *in silico* prediction was employed to estimate molecular characteristics and pharmacological similarities of the target compounds [25].

EXPERIMENTAL

Melting points were determined using a Buchi melting point B-540 instrument and are uncorrected. The purity of the compounds was monitored by TLC plates on silica gel (60 F_{254}) visualized under UV light. In CDCl₃ solution, 100 and 400 MHz spectrometers (Varian 400 MR) were used to record ¹H and ¹³C NMR spectra in tetramethylsilane (TMS) solvent. The IR spectra were recorded on an FT-IR spectrometer (FT/IR-4200, Jasco). Mass spectra were determined using a triple quad-rupole LC-MS (Agilent 6430) at the mass spectroscopy. Chrom-atographic purity was determined using the area normalization method and the corresponding conditions were indicated: flow rate, mobile (range employed), column phase, detection wave-length, *etc*.

Synthesis of 4-hydroxy-1-methyl-6-(prop-2-yn-1-yl-amino)quinolin-2(1H)-one (2): 6-Amino-4-hydroxy-1-methyl-quinolin-2(1H)-one (**1**) (1 g, 0.0052 mol), propargyl bromide (0.45 g, 0.0038 mol) and K₂CO₃ (0.57 g, 0.0042 mol) were combined in a round-bottom flask and dissolved in acetone (10 mL). The mixture was stirred at 30 ºC for 30 min while the reaction progress was monitored by TLC (EtOAc:hexane 1:9). After cooling to the room temperature, the reaction mixture

was poured into 100 mL of ice water, followed by acidification with dilute HCl until a pH = 1 was reached. The resulting product was extracted with ethyl acetate, evaporated under vacuum and dried over anhydrous Na₂SO₄. The obtained solid was further purified by washing with hexane containing 5-10% ethyl acetate.

Synthesis of 2-quinolone bearing 1,2,3-triazoles (4a-f): The key intermediate, 4-hydroxy-1-methyl-6-(prop-2-yn-1-yl-amino)quinolin-2(1H)-one (**2**) (0.5 g, 0.0021 mol) and 4-nitro azidobenzene (**3a**) (0.48 g, 0.0027 mol), were combined in *t*-BuOH:water (5 mL) and treated with copper iodide (0.23 g, 0.0012 mol), triphenyl phosphene (0.33 g, 0.0012 mol) and L-sodium ascorbate (0.24 g, 0.0012 mol) at 45 ºC for 10 min. The conventional technique involved monitoring the reaction progress by TLC (EtOAc:hexane 1:9). Subsequently, the reaction mixture was carefully poured into 50 mL of ice water with conti-nuous stirring. The solid products formed were separated using ethyl acetate (230 mL), followed by filtration and thorough washing with water and a brine solution. The resulting mixture was continuously stirred, resulting in the formation of a solid brown precipitate. The solid precipitate was then subjected to filtration and drying, ultimately yielding the desired compound. To enhance the purity, the obtained residue underwent further purification through washing with a solution of 5-10% ethyl acetate in hexane to give 4-hydroxy-1-methyl-6-(((1-(4-nitro-benzyl)-1H-1,2,3-triazol-4-yl)methyl)amino)quinolin-2(1H)-one (**4a**) (**Scheme-I**).

4-Hydroxy-1-methyl-6-(((1-(4-nitrobenzyl)-1H-1,2,3-triazol-4-yl)methyl)amino)quinolin-2(1H)-one (4a): Yellow crystalline solid, 91% yield, m.p.: 205-207 ºC; IR (KBr, v_{max}, cm⁻¹): 3480.41 (OH), 3392.32 (-NH), 3171.37 (=CH), 2976.23 (-CH), 1776.45 (C=O), 1593.17 (C=C), 1438.74 (C=N), 1279.11 (C-N); ¹H NMR (CDCl₃, 400 MHz) δ ppm: 13.67 (brs, 1H, OH), 8.53 (s, 1H, triazole-H), 7.89 (s, 1H, Ar-H), 8.17 (d, *J* = 7.1 Hz, 2H, Ar-H), 7.41 (d, *J* = 6.9 Hz, 1H, Ar-H), 6.63 (s, 1H, Ar-H), 6.79 (d, *J* = 6.9 Hz, 1H, Ar-H), 4.27 (s, 1H, -NH), 5.28 (s, 2H, -NCH₂), 4.72 (s, 2H, -NCH₂), 3.03 (s, 3H, -NCH₃); ¹³C NMR (CDCl₃, 100 MHz) δ ppm: 165.53 (C₂-CO), 162.86 (C₄), 145.17 (Ar-C), 145.10 (C₆), 139.18 (Ar-C), 136.40 (Ar-C), 133.87 (triazole-C), 132.21 (Ar-C), 130.07 (C₉), 128.03 (triazole-C), 120.72 (C₈), 118.86 (C₇), 111.07 (C₁₀), 110.92 (Ar-C), 106.77 (C₅), 96.67 (C₃), 60.94 (-NCH₂), 45.02 (-NCH₂), 32.92 (-NCH₃); Mass: *m/z* 406 (M)⁺.

6-(((1-(2,4-Dichlorobenzyl)-1H-1,2,3-triazol-4-yl)-methyl)amino)-4-hydroxy-1-methylquinolin-2(1H)-one (4b): White crystalline solid, 91% yield, m.p.: 220-222 ºC; IR (KBr, v_{max}, cm⁻¹): 3410.23 (OH), 3313.28 (NH), 2976.43 (=CH), 2940.57 (-CH), 1736.95 (C=O), 1607.42 (C=C), 1496.79 (C=N), 1420.96 (C-N), 836.04 (C-Cl); ¹H NMR (CDCl₃, 400 MHz) δ ppm: 13.86 (brs, 1H, OH), 8.78 (s, 1H, triazole-H), 8.48 (s, 1H, Ar-H), 7.82 (d, *J* = 6.9 Hz, 1H, Ar-H), 7.43 (d, *J* = 6.9 Hz, 1H, Ar-H), 7.22 (d, *J* = 6.9 Hz, 1H, Ar-H), 6.98 (d, *J* = 6.9 Hz, 1H, Ar-H), 6.77 (s, 1H, Ar-H), 4.26 (s, 1H, -NH), 4.62 (s, 2H, -NCH₂), 3.90 (s, 2H, –NCH₂), 2.88 (s, 3H, -NCH₃); ¹³C NMR (CDCl₃, 100 MHz) δ ppm: 165.86 (C₂-CO), 162.95 (C₄), 148.07 (C₆), 144.89 (Ar-C), 144.82 (Ar-C), 133.79 (Ar-C), 139.15 (Ar-C), 132.30 (triazole-C), 132.14 (C₉), 121.54 (triazole-C),

Scheme-I: Illustrates the conventional synthesis of the desired 2-quinolone–1,2,3-triazole derivatives and their design strategy

119.98 (Ar-C), 118.48 (C_8), 116.96 (C_7), 111.11 (C_{10}), 110.69 (Ar-C), 106.77 (C_5), 96.68 (C_3), 56.94 (NCH_2), 49.25 (NCH_2), 34.34 (NCH_3); Mass: m/z 430 (M)$^+$.

6-(((1-(2-Chlorobenzyl)-1H-1,2,3-triazol-4-yl)methyl)-amino)-4-hydroxy-1-methylquinolin-2(1H)-one (4c): White crystalline solid, 88% yield, m.p.: 191-193 ºC; IR (KBr, ν_{max}, cm^{-1}): 3410.71 (OH), 3252.77 (NH), 2976.20 (=CH), 2940.10 (-CH), 1736.91 (C=O), 1607.87 (C=C), 1496.98 (C=N), 1313.27 (C-N), 836.04 (CCl); ^{1}H NMR (CDCl$_3$, 400 MHz) δ ppm: 12.47 (brs, 1H, OH), 8.33 (s, 1H, triazole-H), 8.02 (s, 1H, Ar-H), 7.61 (d, J = 6.7 Hz, 1H, Ar-H), 7.77 (d, J = 6.9 Hz, 1H, Ar-H), 7.19 (s, 1H, Ar-H), 7.36 (d, J = 7.1 Hz, 2H, Ar-H), 6.99 (t, J = 7.2 Hz, 2H, Ar-H), 4.83 (s, 2H, -NCH$_2$), 4.55 (s, 1H, -NH), 4.01 (s, 2H, -NCH$_2$), 3.22 (s, 3H, -NCH$_3$); ^{13}C NMR (CDCl$_3$, 100 MHz) δ ppm: 164.45 (C_2-CO), 161.58 (C_4), 148.13 (C_6),

143.53 (Ar-C), 143.46 (Ar-C), 138.04 (triazole-C), 133.37 (Ar-C), 131.25 (C_9), 125.43 (triazole-C), 122.17 (C_8), 119.18 (C_7), 116.86 (C_{10}) 111.66 (Ar-C), 109.28 (Ar-C), 106.60 (C_5), 95.45 (C_3), 51.57 (NCH_2), 45.53 (NCH_2), 30.49 (NCH_3); Mass: m/z = 395 (M)$^+$.

4-Hydroxy-1-methyl-6-(((1-(2-methylbenzyl)-1H-1,2,3-triazol-4-yl)methyl)amino)quinolin-2(1H)-one (4d): White solid, 87% yield, m.p.: 191-193 ºC; IR (KBr, ν_{max}, cm^{-1}): 3428.16 (OH), 3310.34 (NH), 3071.67 (=CH), 2946.32 (-CH), 1764.31 (C=O), 1594.11 (C=C), 1456.25 (C=N), 1336.26 (C-N); ^{1}H NMR (CDCl$_3$, 400 MHz) δ ppm: 13.81 (brs, 1H, OH), 8.50 (s, 1H, triazole-H), 8.23 (d, J = 6.9 Hz, 1H, Ar-H), 7.94 (s, 1H, Ar-H), 7.37 (t, J = 7.2 Hz, 2H, Ar-H), 7.20 (s, 1H, Ar-H), 7.67 (d, J = 6.7 Hz, 2H, Ar-H), 6.85 (d, J = 6.8 Hz, 1H, Ar-H), 5.03 (s, 2H, -NCH$_2$), 4.10 (s, 2H, –NCH$_2$), 4.57 (s, 1H, -NH), 3.20

(s, 3H, -NCH₃), 2.86 (s, 3H, CH₃); ¹³C NMR (CDCl₃, 100 MHz) δ ppm: 165.81 (C₂-CO), 162.61 (C₄), 147.22 (C₆), 140.52 (Ar-C), 138.12 (triazole-C), 133.24 (Ar-C), 131.20 (C₉), 125.28 (C₈), 122.34 (triazole-C), 120.64 (C₇), 118.54 (Ar-C) 111.46 (C₁₀), 109.21 (Ar-C), 105.94 (C₅), 96.34 (C₃), 53.46 (-NCH₂), 44.21 (-NCH₂), 30.61 (-NCH₃), 24.15 (-CH₃); Mass: *m/z* = 375 (M)⁺.

4-Hydroxy-1-methyl-6-(((1-(pyridin-4-ylmethyl)-1*H*-1,2,3-triazol-4-yl)methyl)amino) quinolin-2(1*H*)-one (4e): Brown solid, 90% yield, m.p.: 178-180 ºC; IR (KBr, ν_max, cm⁻¹): 3411.76 (OH), 3184.50 (=CH), 2988.94 (-CH), 1751.20 (C=O), 1604.21 (C=C), 1436.53 (C=N), 1314.21 (C-N); ¹H NMR (CDCl₃, 400 MHz) δ ppm: 12.60 (brs, 1H, OH), 8.20 (d, *J* = 7.1 Hz, 2H, Ar-H), 7.86 (d, *J* = 6.9 Hz, 1H, Ar-H), 7.68 (s, 1H, triazole-H), 7.37 (s, 1H, Ar-H), 7.28 (d, *J* = 6.9 Hz, 1H, Ar-H), 7.07 (d, *J* = 7.1 Hz, 2H, Ar-H), 6.81 (s, 1H, Ar-H), 5.34 (s, 2H, -NCH₂), 4.19 (s, 2H, -NCH₂), 4.76 (s, 1H, -NH), 3.01 (s, 3H, -NCH₃); ¹³C NMR (CDCl₃, 100 MHz) δ ppm: 164.61 (C₂-CO), 163.50 (C₄), 158.47 (C₆), 156.27 (Ar-C), 146.08 (Ar-C), 143.62 (triazole-C), 134.70 (Ar-C), 130.07 (C₉), 128.04 (triazole-C), 127.23 (Ar-C), 126.84 (C₈), 124.35 (C₇),123.38 (C₁₀) 119.54 (Ar-C), 116.28 (C₅), 110.17 (C₃), 55.84 (-NCH₂), 38.37 (-NCH₂), 34.89 (-NCH₃); Mass: *m/z* = 362 (M)⁺.

4-Hydroxy-1-methyl-6-(((1-(pyridin-3-ylmethyl)-1*H*-1,2,3-triazol-4-yl)methyl)amino) quinolin-2(1*H*)-one (4f): Brown solid, 86% yield, m.p.: 190-192 ºC; IR (KBr, ν_max, cm⁻¹): 3411.76 (OH), 3184.50 (=CH), 2988.94 (-CH), 1751.20 (C=O), 1604.21 (C=C), 1436.53 (C=N), 1314.21 (C-N); ¹H NMR (CDCl₃, 400 MHz) δ ppm: 13.04 (brs, 1H, OH), 8.22 (d, *J* = 7.1 Hz, 2H, Ar-H), 7.80 (d, *J* = 6.9 Hz, 1H, triazole-H), 7.40 (s, 1H, Ar-H), 7.29 (d, *J* = 6.9 Hz, 1H, Ar-H), 7.05 (d, *J* = 7.1 Hz, 1H, Ar-H), 6.84 (s, 1H, Ar-H), 7.14 (s, 1H, Ar-H), 5.12 (s, 2H, -NCH₂), 4.70 (s, 1H, -NH), 4.10 (s, 2H, -NCH₂), 3.13 (s, 3H, -NCH₃); ¹³C NMR (CDCl₃, 100 MHz) δ ppm: 165.54 (C₂-CO), 163.55 (C₄), 152.25 (Ar-C), 150.43 (Ar-C), 148.40 (C₆), 134.75 (triazole-C), 132.49 (Ar-C), 130.07 (C₉), 129.03 (triazole-C), 128.20 (Ar-C), 126.88 (C₈), 124.45 (C₇),123.30 (Ar-C), 116.37 (C₅), 111.46 (C₃), 54.83 (-NCH₂), 38.34 (-NCH₂), 34.55 (-NCH₃); Mass: *m/z* = 362 (M)⁺.

Synthesis of 2-quinolone bearing 1,2,3-triazoles (6a-f): Key intermediate 4-hydroxy-1-methyl-6-(prop-2-yn-1-yl-amino)-quinolin-2(1*H*)-one (**2**) (0.5 g, 0.0021 mol) and 2-nitro-phenyl-azide (**5a**) (0.44 g, 0.0027 mol) were added in *t*-BuOH:water (1:1) (5 mL). A solution of sodium ascorbate (0.24 g, 0.0012 mol), followed by CuI (0.23 g, 0.0012 mol) and triphenyl phosphene (0.33 g, 0.0012 mol) were added to the reaction mixture and the reaction was refluxed vigorously at 40 ºC. After the reaction was completed, the mixture was poured into 100 mL of ice water and the precipitate was collected by filtration. The purity of solid compound was measured using column chromatography with a solvent system consisting of 10% ethyl acetate in hexane and the desired compound 4-hydroxy-1-methyl-6-(((1-(2-nitrophenyl)-1*H*-1,2,3-triazol-4-yl)methyl)-amino)-quinolin-2(1*H*)-one (**6a**) (**Scheme-I**).

4-Hydroxy-1-methyl-6-(((1-(2-nitrophenyl)-1*H*-1,2,3-triazol-4-yl)methyl)amino)quinolin-2(1*H*)-one (6a): Yellow solid, 91% yield, m.p.: 213-215 ºC; IR (KBr, ν_max, cm⁻¹): 3422.24 (OH), 3106.24 (=CH), 2964.24 (–CH), 1767.36 (C=O),

1601.39 (C=C), 1430.25 (C=N), 1310.67 (C-N); ¹H NMR (CDCl₃, 400 MHz) δ ppm: 13.26 (brs, 1H, OH), 8.63 (d, *J* = 6.9 Hz, 1H, Ar-H), 7.90 (d, *J* = 6.9 Hz, 1H, Ar-H), 7.81 (s, 1H, triazole-H), 7.53 (d, *J* = 7.1 Hz, 2H, Ar-H) 7.34 (s, 1H, Ar-H), 7.05 (d, *J* = 7.1 Hz, 1H, Ar-H), 7.23 (d, *J* = 6.9 Hz, 1H, Ar-H), 6.84 (s, 1H, Ar-H), 4.56 (s, 2H, –NCH₂), 4.10 (s, 1H, -NH), 3.06 (s, 3H, -NCH₃); ¹³C NMR (CDCl₃, 100 MHz) δ ppm: 166.81 (C₂-CO), 162.61 (C₄), 151.22 (Ar-C), 149.36 (C₆), 142.89 (Ar-C), 133.64 (Ar-C), 131.30 (triazole-C), 130.09 (Ar-C), 129.10 (C₉), 128.16 (triazole-C), 125.81 (C₈), 124.40 (C₇),123.27 (Ar-C), 120.29 (C₁₀), 109.37 (C₅), 97.79 (C₃), 40.93 (-NCH₂), 31.22 (-NCH₃); Mass: *m/z* = 392 (M)⁺.

6-(((1-(2,4-Difluorophenyl)-1*H*-1,2,3-triazol-4-yl)-methyl)amino)-4-hydroxy-1-methyl quinolin-2(1*H*)-one (6b): Brownish solid, yield 90%, m.p.: 178-180 ºC; IR (KBr, ν_max, cm⁻¹): 3403.50 (OH), 3200.45 (NH), 2988.94 (-CH), 1751.22 (C=O), 1604.04 (C=C), 1314.21 (C-N), 954.42 (C-F); ¹H NMR (CDCl₃, 400 MHz) δ ppm: 14.01 (brs, 1H, OH), 87.96 (s, 1H, Ar-H),. 61 (s, 1H, triazole-H), 7.43 (d, *J* = 7.1 Hz, 2H, Ar-H), 8.25 (d, *J* = 6.9 Hz, 1H, Ar-H), 6.80 (s, 1H, Ar-H), 7.72 (d, *J* = 6.9 Hz, 1H, Ar-H), 7.21 (d, *J* = 6.9 Hz, 1H, Ar-H), 5.02 (s, 1H, -NH), 4.58 (s, 2H, -NCH₂), 3.07 (s, 3H, -NCH₃); ¹³C NMR (CDCl₃, 100 MHz) δ ppm: 167.17 (C₂-CO), 166.14 (Ar-C), 164.91 (C₄), 154.64 (Ar-C), 145.91 (C₆), 139.80 (triazole-C), 139.83 (Ar-C), 138.20 (C₉), 137.55 (C₈), 132.97 (triazole-C), 121.84 (Ar-C), 119.94 (C₇), 112.63 (C₁₀), 111.48 (Ar-C), 108.23 (C₅), 104.99 (Ar-C), 97.12 (C₃), 42.35 (-NCH₂), 28.36 (-NCH₃); Mass: *m/z* 383 (M)⁺.

6-(((1-(4-Chlorophenyl)-1*H*-1,2,3-triazol-4-yl)methyl)-amino)-4-hydroxy-1-methylquinolin-2(1*H*)-one (6c): Brownish solid, yield 91%, m.p.: 208-210 ºC; IR (KBr, ν_max, cm⁻¹): 3411.76 (OH), 3249.34 (NH), 2982.91 (-CH), 1748.94 (C=O), 1607.10 (C=C), 1429.02 (C=N), 1282.23 (C-N), 841.76 (C-Cl); ¹H NMR (CDCl₃, 400 MHz) δ ppm: 13.34 (brs, 1H, OH), 8.48 (s, 1H, triazole-H), 8.19 (d, *J* = 6.9 Hz, 1H, Ar-H), 7.52 (d, *J* = 6.9 Hz, 1H, Ar-H), 7.75 (d, *J* = 7.1 Hz, 2H, Ar-H), 7.27 (d, *J* = 7.1 Hz, 2H, Ar-H), 7.03 (s, 1H, Ar-H), 5.45 (s, 1H, -NH), 5.20 (s, 2H, -NCH₂), 3.41 (s, 3H, -NCH₃); ¹³C NMR (CDCl₃, 100 MHz) δ ppm: 167.89 (C₂-CO), 167.19 (C₄), 147.54 (Ar-C), 144.59 (Ar-C), 142.93 (C₆), 138.93 (triazole-C), 132.55 (Ar-C), 131.58 (C₈), 129.93 (C₉), 128.33 (triazole-C), 122.17 (Ar-C), 119.94 (C₇), 118.86 (C₁₀), 117.06 (Ar-C), 112.44 (Ar-C), 108.19 (C₅), 93.82 (C₃),54.16 (-NCH₂), 35.86 (-NCH₃); Mass: *m/z* 381 (M)⁺.

4-Hydroxy-1-methyl-6-(((1-(4-(trifluoromethyl)-phenyl)-1*H*-1,2,3-triazol-4-yl)methyl)amino) quinolin-2(1*H*)-one (6d): Brown solid, yield 86%, m.p.: 167-169 ºC; IR (KBr, ν_max, cm⁻¹): 3410.23 (OH), 3252.73 (NH), 2976.42 (=CH), 2940.57 (-CH), 1736.95 (C=O), 1607.42 (C=C), 1420.96 (C=N), 1313.28 (C-N), 1020.71 (C-F); ¹H NMR (CDCl₃, 400 MHz) δ ppm: 13.77 (brs, 1H, OH), 8.29 (s, 1H, triazole-H), 7.64 (s, 1H, Ar-H), 7.86 (d, *J* = 6.9 Hz, 1H, Ar-H), 7.18 (d, *J* = 7.0 Hz, 1H, Ar-H), 7.02 (d, *J* = 7.1 Hz, 2H, Ar-H), 7.32 (d, *J* = 7.2 Hz, 2H, Ar-H), 6.83 (s, 1H, Ar-H), 4.78 (s, 2H, -NCH₂), 4.81 (s, 1H, -NH), 2.78 (s, 3H, –NCH₃); ¹³C NMR (CDCl₃,100 MHz) δ ppm: 165.77 (C₂-CO), 162.53 (C₄), 144.96 (C₆), 146.31 (Ar-C), 138.46 (Ar-C), 134.24 (triazole-C), 131.16 (C₉), 131.11 (Ar-C), 124.14 (Ar-C), 122.50 (Ar-C), 124.14 (C₈), 122.50 (triazole-C), 121.22

(Ar-C), 117.82 (C_9), 115.20 (C_7), 113.05 (Ar-C),108.23 (C_{10}), 104.94 (C_5), 98.22 (C_3), 55.74 (-NCH$_2$), 34.44 (-NCH$_3$); Mass: m/z 415 (M)$^+$.

4-Hydroxy-1-methyl-6-(((1-(pyridin-4-yl)-1H-1,2,3-triazol-4-yl)methyl)amino)quinolin-2(1H)-one (6e): Brown solid, yield 89%, m.p.: 184-186 ºC; IR (KBr, v_{max}, cm^{-1}): 3448.66 (OH), 3392.96 (-NH), 3176.80 (=CH), 2976.88 (-CH), 1736.23 (C=O), 1593.45 (C=C), 1438.36 (C=N), 1279.84 (C-N); ^{1}H NMR (CDCl$_3$, 400 MHz) δ ppm: 12.61 (brs, 1H, OH), 8.34 (d, J = 7.1 Hz, 2H, Ar-H), 8.09 (s, 1H, triazole-H), 7.88 (d, J = 6.9 Hz, 1H, Ar-H), 7.58 (s, 1H, Ar-H), 7.52 (d, J = 7.0 Hz, 1H, Ar-H), 7.37 (d, J = 7.1 Hz, 2H, Ar-H), 7.22 (s, 1H, Ar-H), 4.77 (s, 2H, –NCH$_2$), 4.18 (brs, 1H, -NH), 3.08 (s, 3H, -NCH$_3$); ^{13}C NMR (CDCl$_3$, 100 MHz) δ ppm: 163.37 (C_2-CO), 161.91 (C_4), 156.34 (Ar-C), 148.31 (Ar-C), 145.40 (C_6), 144.52 (Ar-C), 132.93 (triazole-C), 131.81 (C_9), 128.54 (Ar-C), 127.28 (Ar-C), 126.94 (Ar-C), 126.77 (C_8), 124.32 (triazole-C), 123.41 (Ar-C), 121.83 (C_9), 111.81 (C_7), 53.37 (NCH$_2$), 35.17 (NCH$_3$); Mass: m/z 348 (M)$^+$.

4-Hydroxy-1-methyl-6-(((1-(p-tolyl)-1H-1,2,3-triazol-4-yl)methyl)amino)quinolin-2(1H)-one (6f): White solid, yield 88%, m.p.: 170-172 ºC; IR (KBr, v_{max}, cm^{-1}): 3430.15 (OH), 3107.31 (=CH), 2950.48 (-CH), 1737.20 (C=O), 1555.12 (C=C), 1443.18 (C=N), 1346.21 (C-N); ^{1}H NMR (CDCl$_3$, 400 MHz) δ ppm: 14.12 (brs, 1H, OH), 8.54 (s, 1H, triazole-H), 8.23 (d, J = 6.9 Hz, 1H, Ar-H), 8.04 (s, J = 7.1 Hz, 2H, Ar-H), 7.55 (d, J = 7.1 Hz, 2H, Ar-H), 7.74 (s, 1H, Ar-H), 6.89 (s, 1H, Ar-H), 7.26 (d, J = 6.9 Hz, 1H, Ar-H), 4.60 (s, 2H, -NCH$_2$), 4.21 (s, 1H, -NH), 3.29 (s, 3H, -NCH$_3$), 2.67 (s, 3H, CH$_3$); ^{13}C NMR (CDCl$_3$, 100 MHz) δ ppm: 164.21 (C_2-CO), 161.30 (C_4), 152.22 (C_6), 146.61 (Ar-C), 135.30 (Ar-C), 134.83 (triazole-C), 132.70 (C_9), 128.52 (Ar-C), 130.31 (Ar-C), 126.34 (Ar-C), 122.37 (triazole-C), 120.43 (C_8), 119.20 (C_7), 114.55 (C_{10}), 112.40 (C_5), 95.64 (C_3), 43.91 (-NCH$_2$), 32.50 (-NCH$_2$), 24.25 (-NCH$_3$); Mass: m/z 361(M)$^+$.

Bacterial strains and growth conditions: *Staphylococcus epidermidis*, *Staphylococcus aureus*, *Pseudomonas aeruginosa*, *Aspergillus clavatus*, *Aspergillus niger* and *Candida albicans* strains were grown as described by using agar dilution methods [26]. Disks were allowed to dry for 20 min, and then stored in a sealed bag with desiccant at 4 ºC. Growth from 4-day old plates was resuspended in 1.0 mL sterile Heart Infusion Broth, and turbidity was adjusted to a McFarland 2.0 by visual inspection. The bacterial suspension was spread over the surface of a chocolate agar plate using a swab. The inoculum was allowed to dry into the agar in a biological safety cabinet for 15 min. Disks were then placed in the centre of plates, which were inverted and incubated at 37 ºC in a 5% CO$_2$ incubator for one week. For all organisms, the zone of inhibition was measured by recording the diameter, to the nearest mm, for each disk. Briefly, strains were tested for growth on chocolate agar plates containing antibiotics at 50, 25, 12.5, 10 and 1.5 µg/mL. Compounds inhibiting growth at 50 µg/mL were further tested to determine the more precise MIC using 2-fold dilutions at and below 1.5 µg/mL. Agar plates containing DMSO (without compound) as a control were prepared at the highest dilution to assess any antibacterial activity associated with the solvent.

Growth from four-day old chocolate agar plates was collected for each Bartonella strain tested. The growth was suspended into 0.5 mL of sterile Heart Infusion broth. The turbidity was adjusted to a McFarland standard of 2.0 by visual comparison to turbidity standards. Inoculation drops were allowed to briefly dry into the agar. Plates were inverted and incubated at 37 ºC with a 5% CO$_2$ atmosphere for 7 days. Growth was recorded as positive or for each strain on duplicate plates.

Molecular docking studies: All the synthesized molecules were sketched in ACD chemsketch and saved it in .mol file. Later all the sketched molecules were converted to pdb format using OPENBABEL software. The "Crystal structure of sterol 14-α demethylase (CYP51) from *Candida albicans* in complex with the tetrazole-based antifungal drug candidate VT1161 (VT1) was downloaded from RCSB, a protein structure database. The prepared protein and ligands were used as input files for AutoDock 4.2 in the next step. The standard docking procedure was used for a rigid protein and a flexible ligand whose torsion angles were identified. Protein was prepared by adding hydrogen bonds and also ligands were also prepared individually. A grid of 60, 60, and 60 points in x, y and z directions was built with a grid spacing of 0.375 Å and a distance-dependent function of the dielectric constant were used for the calculation of the energetic map. The default settings were used for all other parameters. Lamarckian genetic algorithm method was employed for docking simulations. At the end of docking, the best poses were analyzed for the hydrogen bonding calculations using Autodock 4.2. From the estimated free energy of ligand binding (ΔG$_{binding}$, kcal/mol), the inhibition constant (K_i) for each ligand was calculated.

RESULTS AND DISCUSSION

In present study, it was required to examine the suitability of copper catalysts for the synthesis of the desired substituted 2-quinolone-1,2,3-triazole derivatives (**Scheme-I**). Substituted azides was synthesized according to published procedure [27]. Accordingly, the reaction of 4-hydroxy-1-methyl-6-(prop-2-yn-1-ylamino)quinolin-2(1H)-one (**2**) with 1-(azidomethyl)-4-nitrobenzene (**3a**) was investigated under various conditions (Table-1) [28]. A solution of CuI/PPh$_3$ in DMSO was used for carrying out the following reaction for 30 min, the temperature was maintained at 40 ºC.

The reaction proceeded efficiently, resulting in the expected product **4a** with a commendable 78% yield under standard conditions (entry 1, Table-1). Solvent variations, such as switching from DMSO to chloroform (entry 2, Table-1) or DCM (entry 3, Table-1), exhibited no significant influence on the yield. However, the use of DCM:water (1:1) as the solvent led to a substantial increase in yield, reaching 88% (entry 3, Table-1). Exploring alternative conditions, the reaction was conducted in acetonitrile at 40 ºC, resulting in a remarkable 77% improvement in product yield, exibhiting the sensitivity of the process to reaction conditions (entry 4, Table-1). Additionally, after 20 min of refluxing in water, the addition of DMF produced the desired product with a yield of 73% (entry 5, Table-1). This was favourable and the reaction time was raised to 45 min to optimize the product yield further. However, using ethanol as a

TABLE-1
THE REACTION CONDITIONS OF QUINOLONE BASED 1,2,3-TRIAZOLE DERIVATIVES (**2,3a**)[a]

Entry	Solvent	Catalyst	Temp. (°C)	Time (min)	Yield (%)[b]
1	DMSO	CuI	40	30	78
2	CHCl$_3$	CuI	40	30	86
3	DCM:H$_2$O	CuI	40	30	88
4	ACN	CuI	40	20	77
5	DMF	CuI	40	20	73
6	EtOH	CuI	40	45	85
7	Propanol	CuI	50	45	76
8	MeOH	CuI	45	20	80
9	*t*-BuOH	CuI	45	45	90

[a]All the reactions were performed using **2** (0.0021 mol), **3a** (0.0027 mol) and a catalyst (0.0012 mol) in a solvent (5 mL) in the presence of ultrasound in the open air; [b]Isolated yield; [c]The reaction was carried out without ultrasound irradiation.

solvent did not significantly increase yield (entry 6, Table-1). Elevating the reaction temperature to 50 °C in the presence of propanol resulted in an increased yield of 76% (entry 7, Table-1). Although the remarkable improvement, product **4a** was successfully synthesized in methanol, employing CuI/PPh$_3$ as catalysts, with a satisfactory yield of 80%. Consequently, the reaction was conducted both with and without a catalyst. In first case, the yield of product **4a** decreased (entry 8, Table-1). Intriguingly, the reaction also took place without the application of heating conditions, resulting in the formation of product **4a**, albeit at a lower yield. Subsequently, the catalyst loading, specifically the necessity for using CuI in all these reactions, was investigated. Furthermore, the high yield of the product have obtained by using of *t*-BuOH:H$_2$O (entry 9, Table-1). Hence, the optimization reaction conditions of the reaction *t*-BuOH: H$_2$O as a solvent in presence of CuI catalyst at 45 °C for 45 min to gave 90% of the yield. After the reaction was completed, water was added to the reaction mixture to the separate the organic and aqueous layers. The organic layer was then subjected to drying, filtration and subsequent washing with acetone, aimed at removing impurities and obtaining a purified product. The purification steps are essential to ensure the isolation of high-quality product **4a**. After the revelation of copper as a catalyst in the synthesis of the newly formed compound **4a** using *t*-BuOH and water, it became imperative to explore and define the applicability and substrate scope of this synthetic method. The focus extended beyond the initial compound to include the generation of analogues of **4a**, prompting further studies to broaden the understanding of the synthetic process.

Consequently, employing various substrates, the process was investigated for the formation of diverse quinolone-based 1,2,3-triazole derivatives (**4a-f** & **6a-f**). On the benzene ring, for instance, azides **3** having mild to strong electron-releasing groups such as -OCH$_3$, -CH$_3$ and –Cl, as well as strong electron-withdrawing moieties such as -NO$_2$, -F, *etc.* have been used. The chemical structures of the quinolones containing 1,2,3-triazole **4** and **6** were characterized using ^{1}H NMR, ^{13}C NMR, IR and mass spectroscopy techniques. The ^{1}H NMR spectrum of triazole hybrid **4a** showed a singlet peak at δ 7.32, 1.54 ppm. The -OH protons of the quinolone and triazole functionalities resonance peaks showed at δ 13.67, 8.53 ppm. The quinolone protons a doublet peak showed at δ 7.41 and 6.79 ppm. 4-nitrobenzene substituents two doublets peak showed at δ 8.17 and 7.18 ppm, the quinolone proton a singlet peak at δ 7.89 ppm and corresponds to the methylene protons of -NCH$_2$, -NCH$_3$ a singlet at δ 5.28, 4.72, 3.03 ppm, respectively.

The IR spectrum of compound **4a** shows peak at 3392.32 cm^{-1} and 3480.41 cm^{-1} are related to -NH and -OH stretching bands, respectively. The different characteristic frequencies at 1736.45 and 1593.17 cm^{-1} was corresponded to -C=O and -C=C functional groups, while the characteristic intensity peaks at 3171.37 and 2976.23 cm^{-1} are related to =CH and -CH frequencies. Another support for the closure of the quinolone linked 1,2,3-triazole was the development of the quinolone -CO peak at δ 165.53 and δ 162.86, 145.10 ppm belongs to C$_4$ and C$_6$ carbons, respectively. Another remarkable feature of the ^{13}C NMR spectra of this triazole are the peaks in the downfield region at δ 145.17-110.92 ppm, which show the existence of aromatic carbons and the signals at 128.03, 106.77 and 96.67 ppm clearly show the existence of triazole, C$_5$ and C$_3$ carbon groups. Finally, the signals detected at 60.94, 45.02 and 32.92 ppm are because of the presence of -NCH$_2$, -NCH$_2$ and -NCH$_3$ carbons, respectively. Furthermore, the compound showed a molecular ion peak at *m/z*: 406 [M]$^+$, confirming the structure of 4-hydroxy-1-methyl-6-((((1-(4-nitrobenzyl)-1*H*-1,2,3-triazol-4-yl)methyl)amino)-quinolin-2(1*H*)-one (**4a**).

Antimicrobial activity: The agar-well diffusion method was employed to assess the antibacterial and antifungal activities of the compounds. Specifically, the study included Gram-positive bacteria *i.e.*, *S. epidermidis*, *S. aureus*, one Gram-negative *i.e.*, *P. aeruginosa*, as well as three antifungal activity *i.e. A. clavatus*, *A. niger* and *C. albicans* [29,30]. Compounds **4a**, **4f**, **6d** and **6e** exhibited significant effectiveness against all the tested microorganisms, with MIC values ranging from 2.28 to 10.81 µg/mL. It is found that the synthesized compounds demonstrated the superior efficacy compared to the common antibiotic moxifloxacin (MIC = 2.55-3.24 µg/mL) against the same microorganisms (Table-2).

The results indicate varied inhibitory effects of the tested compounds, with MIC values against Gram-positive bacteria ranging from 43.42-2.28 µg/mL. For Gram-negative bacteria, the MIC values ranged from 33.91-3.19 µg/mL unexpectedly *ortho*-substitution of the phenyl ring increases with 1,2,3-triazole moieties of **4a** (4-nitophenyl methyl), **4f** (pyridin-3-yl methyl), **6d** (4-trifluoromethyl phenyl) and **6a** (2-nitrophenyl) improved the antimicrobial activity by 2-6 times. In general, the synthesized triazoles **6d**, **4f** and **6a** demonstrated excellent activity against bacterial strains *i.e.*, *S. epidermidis* with MICs of 2.38 ± 0.01, 5.18 ± 0.03 and 6.32 ± 0.04 µg/mL, respectively, whereas indazoles **4d**, **6a** and **4e** demonstrated moderate to good activity against bacterial strains *i.e.*, *S. epidermidis* with MICs of 10.37 ± 0.02, 14.33 ± 0.01, 16.50 ± 0.01 µg/mL. Specifically, compounds **6e**, **6d**, **4f** and **4e** demonstrated a broad-spectrum antimicrobial activity with MIC values of 13.43 ± 0.03, 3.32 ± 0.04, 4.18 ± 0.02 and 2.28 ± 0.01 µg/mL, against Gram-positive bacteria *S. aureus*. In contrast, even at the highest concentration used, 50 µg/mL, compounds **4b**, **4a**, **6e** and **6b** did not prevent the development of *S. epidermidis* and *S. aureus*. Thus, targets **4a**, **4b**, **4f** were identified as they exhibited antibacterial activity against *P. aeruginosa* with respective MIC values of 4.44 ± 0.01, 3.19 ± 0.04, 6.13 ± 0.03 µg/mL, while, these triazole **6e**, **6c** and **4e** showed the identical antibacterial activity against *P. aeruginosa*, the specific MIC values of 12.55 ± 0.03, 16.51 ±

0.02 and 11.81 ± 0.03 µg/mL compared to the reference moxifloxacin (2.63 ± 0.04 µg/mL). In case of Gram-positive bacteria, compounds **4a**, **4f**, **6d** and **6e** demonstrated more effective antibacterial activity against both strains *S. epidermidi*, *S. aureus* with MICs ranging from 2.28 ± 0.01 to 6.32 ± 0.04 µg/mL compared to the reference moxifloxacin 2.97 ± 0.03 to 2.55 ± 0.01 µg/mL. Most of the compounds showed moderate to good antibacterial activity against both Gram-positive and Gram-negative bacteria.

In addition, compounds **6d**, **4a**, **6e** and **4f** showed significant inhibitory antifungal activity against *A. clavatus* with MIC values of 2.52 ± 0.01, 10.18 ± 0.03, 10.81 ± 0.03 and 2.88 ± 0.02 µg/mL. The final 1,2,3-triazoles **4d** (2-methylphenyl methyl), **4b** (2,4-dichlorophenyl methyl) and **6b** (2,4-difluoro phenyl) show moderate to good activity against fungal strains *i.e. A. clavatus* fungal microorganisms with their MIC values of 23.25 ± 0.01, 23.72 ± 0.04, 22.66 ± 0.03 µg/mL. In addition, triazoles **6d**, **4f**, **4c** and **6e** showed the more strongest antifungal activity against fungal strains *i.e.*, *A. niger* with MIC values 4.10 ± 0.03, 7.19 ± 0.03, 2.67 ± 0.01 and 5.49 ± 0.02 µg/mL respectively, However compounds **4a**, **4c** and **6a** exhibited no antifungal activity against *A. niger*. The fungal strain *i.e.*, *C. albicans* demonstrated resistance to the new triazole derivatives **6d**, **4f**, **4c** and **4a**, which generated an interesting effect with MIC values of 3.74 ± 0.03, 3.16 ± 0.02, 4.18 ± 0.03 and 2.70 ± 0.01 µg/mL, which are much greater than those of the standard drug fluconazole (2.92 ± 0.01 to 3.06 ± 0.03 µg/mL). The antifungal activity of the final compounds **6e**, **4b**, **6a**, **4e** and **6f** against *i.e. C. albicans* have only moderate to good with their MICs of 12.19 ± 0.02, 13.25 ± 0.01, 17.63 ± 0.02, 19.55 ± 0.04 and 30.11 µg/mL, respectively.

In silico studies

Docking studies: Molecular modeling techniques were employed for the target compounds against the catalytic core of *Staphylococcus aureus* DNA gyrase complex (PDB: 2XCO) with a 3.1A crystal structure. Autodock 4.2 was used for docking

TABLE-2
ANTIBACTERIAL AND ANTIFUNGAL ACTIVITIES OF THE FINAL
2-QUINOLONE LINKED TO 1,2,3-TRIAZOLE MOIETY WERE EVALUATED

Entry	Bacterial strains[a]				Fungal strains	
	S. epidermidis	*S. aureus*	*P. aeruginosa*	*A. clavatus*	*A. niger*	*C. albicans*
4a	6.32 ± 0.04	> 50	3.19 ± 0.04	2.88 ± 0.02	> 50	4.18 ± 0.03
4b	> 50	> 50	4.44 ± 0.01	23.25 ± 0.01	24.23 ± 0.01	13.25 ± 0.01
4c	19.15 ± 0.01	16.42 ± 0.02	12.55 ± 0.03	> 50	5.49 ± 0.02	3.16 ± 0.02
4d	10.37 ± 0.02	15.42 ± 0.01	> 50	22.66 ± 0.03	30.49 ± 0.04	> 50
4e	16.50 ± 0.01	13.43 ± 0.03	16.51 ± 0.02	> 50	34.30 ± 0.03	19.55 ± 0.04
4f	5.18 ± 0.03	4.18 ± 0.02	6.13 ± 0.03	10.81 ± 0.03	4.10 ± 0.03	3.74 ± 0.03
6a	14.33 ± 0.01	17.47 ± 0.04	> 50	> 50	> 50	17.63 ± 0.02
6b	> 50	> 50	33.91 ± 0.01	23.72 ± 0.04	44.70 ± 0.04	24.19 ± 0.01
6c	43.42 ± 0.02	26.82 ± 0.02	> 50	37.51 ± 0.02	> 50	34.73 ± 0.01
6d	2.38 ± 0.01	3.32 ± 0.04	8.71 ± 0.01	2.52 ± 0.01	2.67 ± 0.01	2.70 ± 0.01
6e	> 50	2.28 ± 0.01	11.81 ± 0.03	10.18 ± 0.03	7.19 ± 0.03	12.19 ± 0.02
6f	20.23	16.48	> 50	25.78	> 50	30.11
MXF[b]	2.55 ± 0.01	2.97 ± 0.03	2.63 ± 0.04	ND	ND	ND
FLZ[c]	ND	ND	ND	3.06 ± 0.03	3.24 ± 0.02	2.92 ± 0.01

[a]MIC = Minimum inhibitory concentration (µg/mL); [b]MXF = Moxifloxacin, FLZ[c] = Fluconazole has been used in discs as a positive reference standard. > 50: not active; ND: Not done; ± mean values.

simulations [31-34]. The co-crystallized ligand (moxifloxacin) was used as a reference molecule. The reported key binding site of the DNA gyrase complex involves MetA:1179, GlyA: 1178, AlaA:1180, ThrA:1181, LeuA:1085, GlyA:1174, AlaA: 1034, AlaA:1172, GlnA:1267, SerA:1098, SerA:1173, PheA: 1266, TyrA:1099, ProA:1036, LeuA:1042, GlyA:1171, LysA: 1043, ArgA:1092, HisA:1046, ProA:1185 and GlyA:1041. All docked molecules were inserted between the neighbouring nucleotides at the active site and stabilized by various interactions. The docking study results demonstrated that the docked compounds had a comparable binding mechanism to the reference ligand moxifloxacin (MXF) and the docked compounds

binding energies are reported in Table-3. Regarding compound **4a**, the planar aromatic system was inserted between the neighbouring nucleotides of DNA gyrase resulting in the formation of seven hydrophobic stackings with amino acid residues ArgA:1092, PheA:1266, LysA:1043, AlaA:1172, AlaA:1034, TyrA:1099, HisA:1046. The terminal nitrobenzene moiety bound the minor groove of DNA forming one hydrophobic interaction with amino acid residue AlaA:1034. Moreover, the 1,2,3-triazole moiety was oriented into the minor groove, resulting in two hydrophobic interactions with LysA:1043, AlaA:1172 (Fig. 1a). According to the outcomes in Table-3, all investigated compounds demonstrated promising Autodock

TABLE-3
DIFFERENT DOCKING POSES INTERACT WITH THE ANTIBACTERIAL DRUG
CANDIDATE *S. aureus* AND THE 2XCO PROTEIN IN A DNA COMPLEX

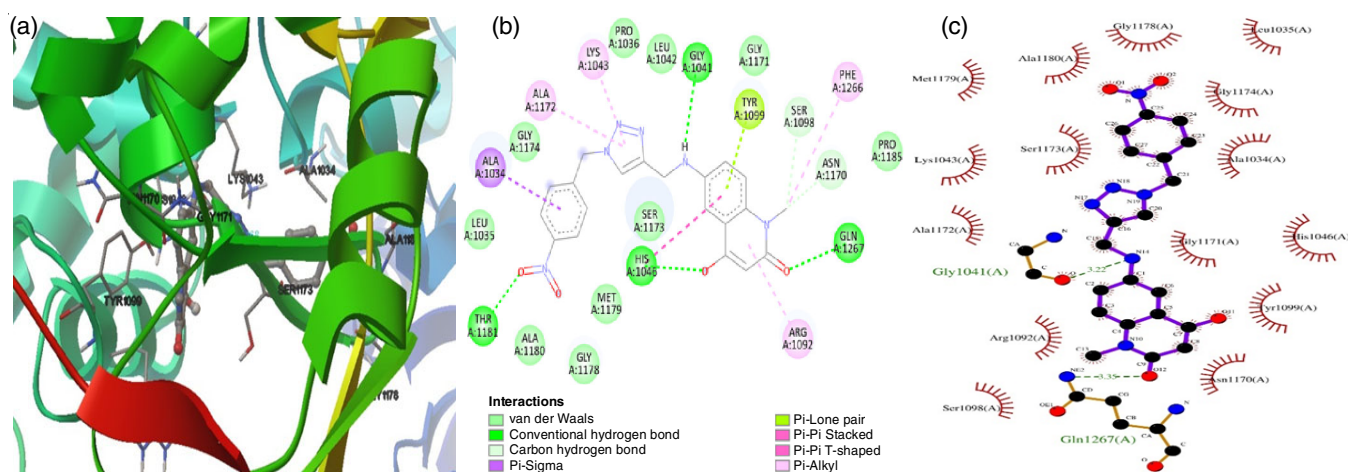| Entry	ΔG (Kcal/mol)/(kl)	Interacting amino acids	Bond distance
4a	−10.25/30.53 nM	Hydrogen bondings: GlyA:1041, HisA:1046, GlnA:1267, ThrA:1181 Carbon hydrogen bondings: TyrA:1099, AlaA:1034, SerA:1173 Pi-alkyl residues: ArgA:1092, PheA:1266, LysA:1043, AlaA:1172 Pi-sigma: AlaA:1034 Pi-lone pair: TyrA:1099 Pi-Pi: HisA:1046 van der Waals forces: ProA:1036, LeuA:1042, GlyA:1171, ProA:1185, GlyA:1174, SerA:1173, MetA:1179, GlyA:1178, AlaA:1180	3.22 Å, 3.10 Å 3.35 Å, 2.86 Å 3.46 Å
6d	−8.69/423.53 nM	Hydrogen bondings: GlyA:1041, SerA:1173 Carbon hydrogen bondings: AsnA:1170, SerA:1098, AlaA:1034 Pi-alkyl residues: LysA:1043, ProA:1036, ArgA:1092 Pi-sigma: AlaA:1034, AlaA:1172, TyrA:1099 Halogenated bonds: GlyA:1174, GlyA:1178 X 2 Pi-Pi: HisA:1046, TyrA:1099 van der Waals forces: LeuA:1035, ThrA:1181, AlaA:1180, MetA:1179, SerA:1173, LeuA:1042, GlyA:1171, GlnA:1267	3.13 Å, 2.61 Å 3.07 Å, 1.89 Å
6e	−8.96/269.29 nM	Hydrogen bondings: AsnA:1170, AlaA:1180, ThrA:1181, SerA:1173, GlnA:1267 Carbon hydrogen bondings: SerA:1173, HisA:1046, TyrA:1099 Pi-alkyl residues: ArgA:1092 X 3, AlaA:1172, LysA:1043, ProA:1036, AlaA:1180 Pi-sigma: AlaA:1034, ThrA:1181 Pi-Pi: TyrA:1099 X2 van der Waals forces: ProA:1185, GlyA:1171, SerA:1098, PheA:1266, GlyA:1174, MetA:1179, LeuA:1035	2.71 Å, 2.82 Å, 2.46 Å, 2.86 Å, 2.99 Å 2.46 Å, 2.83 Å
MXF	−8.10/213.67 nM	Hydrogen bondings: AlaB:11SerA:1098, MetA:1179 Pi-alkyl residues: SerA:1172, AlaA:1034, SerA:1085 Pi-Pi: GlyA:1043 van der Waals forces: ThrA:1182, AlaA:1180, SerA:1173, LeuA:1042, GlyA:1171	2.49 Å, 2.98 Å, 2.10 Å 2.64 Å

Fig. 1a. (a) 3D-structures, (b) 2D-structures and (c) Ligplot images

scores against DNA gyrase with values of –8.69 to –10.25 Kcal/mol and dissociate constant values from 30.53 nM to 423.53 nM, respectively. The 2-quinalone moiety of compound **4a** formed one pi-pi interaction with HisA:1046 with bond distance 3.46 Å, whereas this core was forming two hydrogen bonding interactions with amino acids HisA:1046 [O11···NH], GlnA:1267 [O12···NE2] with their bond distance 3.10 Å, 3.35 Å respectively. The –NH group of **4a** created one hydrogen bond with GlyA:1041 [N14···O, 3.22 Å] and the nitrobenzene moiety of this ligand exhibited one hydrogen bond with ThrA: 1181 [O1···N]. The groups of ProA:1036, LeuA:1042, GlyA: 1171, ProA:1185, GlyA:1174, SerA:1173, MetA:1179, GlyA: 1178 and AlaA:1180residues were identified as contributing to the formation of a pocket around **4a** through van der Waals forces.

Significantly compound **6d** exhibited two hydrogen bonds with GlyA:1041 (N14···O, 3.13 Å) and SerA:1173 (N18···NH, 2.61 Å) inside the active sites of *S. aureus* from DNA Gyrase. More exactly, this ligand exhibited three pi-sigma bondings with amino acid residues AlaA:1034, AlaA:1172, TyrA:1099 and three carbon hydrogen bondings with TyrA:1099, AlaA: 1034, SerA:1173 inside the binding pockets of antibacterial protein 2XCS (Fig. 1b). When the binding mechanisms were examined, it was discovered that compound **6d** generated three pi-alkyl interacting amino acid residues with LysA:1043, ProA:1036, ArgA:1092 inside the binding pockets of DNA gyrase. Other interactions exhibits Pi-Pi bondings with HisA: 1046 (quinolone moiety, 3.07 Å), TyrA:1099 (quinolone moiety, 1.89 Å) and pi-lone pair or unfavourable accepter-accpeter binding with TyrA:1099 amino acid. Furthermore, three hydrogen bonding interactions were observed between F31 and the amino group of glycine. (GlyA:1174, 2.07 Å) and F29 X 2 with oxygen of glycine (GlyA:1178, 1.90, 1.87 Å). This compound also established van der Waals binding contacts with LeuA: 1035, ThrA:1181, AlaA:1180, MetA:1179, SerA:1173, LeuA: 1042, GlyA:1171, GlnA:1267 in complex with 2XCS substituents *via* the active site pocket of *S. aureus*.

Docking interactions of target compound **4a** with the active site of *S. aureus* DNA Gyrase complex [PDB: 2XCO]. Compound binding mode (lime colour) at the moving site of a *S. aureus*

subunit; hydrogen bond interactions are represented as dotted lines, light-green, important residues are represented in light/bluecyan and a protein cartoon is illustrated based on the secondary protein structure.

The most active ligand **6e**, which is found highest hydrogen bonding interactions for adopted by the co-crystallized ligand binding to the active site amino acids including AsnA:1170 [O13···O, 2.71 Å], AlaA:1180 [N25···N, 2.82 Å], ThrA: 1181 [N25···O, 2.46 Å], SerA:1173 [N19···N, 2.86 Å], GlnA:1267 [O12···NE2, 2.99 Å], which interacts with the quinolone, triazole, pyridine ring for **6e** (Fig. 1c). Also, this ligand shows hydrophobic interactions like pi–pi stackings with TyrA:1099 X 2, two pi-sigma interacting amino acids AlaA:1034, ThrA: 1181 with 2-quinolone ring and pyridine pocket residue. The docking study revealed that the most active compound **6e** the exhibited strong van der Waals interactions with amino acid residues ProA:1185, GlyA:1171, SerA:1098, PheA:1266, GlyA:1174, MetA:1179, LeuA:1035, forming a strong association within the active site of DNA gyrase. Furthermore, it established carbon-hydrogen bonding interactions with crucial amino acids, including SerA:1173, HisA:1046 and TyrA:1099.

Moreover, the docking score of compound **6e** [ΔG = –8.96 kcal/mol] demonstrated an increased inhibitory effect, attributed to the formation of seven pi-alkyl bonds with amino acids ArgA:1092 (three interactions), AlaA:1172, LysA:1043, ProA:1036 and AlaA:1180 within the active site of the 2XCS protein. The reference MXF exhibited distinct and significant hydrogen bonding interactions with amino acids in the mobile site, specifically AlaB:11, SerA:1098, MetA:1179, with bond distances of 2.49 Å, 2.98 Å and 2.10 Å, respectively. Whereas the ligand exhibited other amino acids like pi-pi stackings with amino acid GlyA:1043 (2.64 Å) and pi-alkyl interactions with SerA:1172, AlaA:1034, SerA:1085 amino acids respectively. The carbon-hydrogen bond (aqua), hydrogen bonds stackings (green), pi-alkyl (rose), sigma stackings (rose), pi-sulphur (yellow), pi-anion (dark orange), pi-sigma (violet), pi-halogen (blue) and pi-pi (pink) were discovered.

ADMET properties: Reliable online programs such as ADMET lab2.0 and Swiss ADME predict the similarity of substances to drugs and their behaviour in the body [35-37].
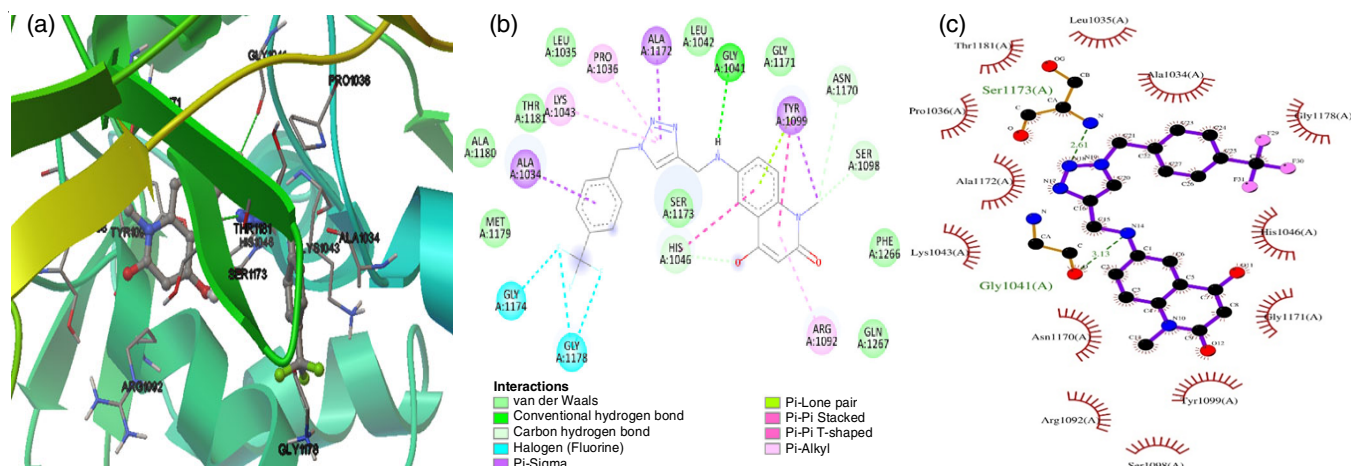

Fig. 1b. (a) 3D-structure, (b) 2D-structure and (c) Ligplot image of ligand **6d**
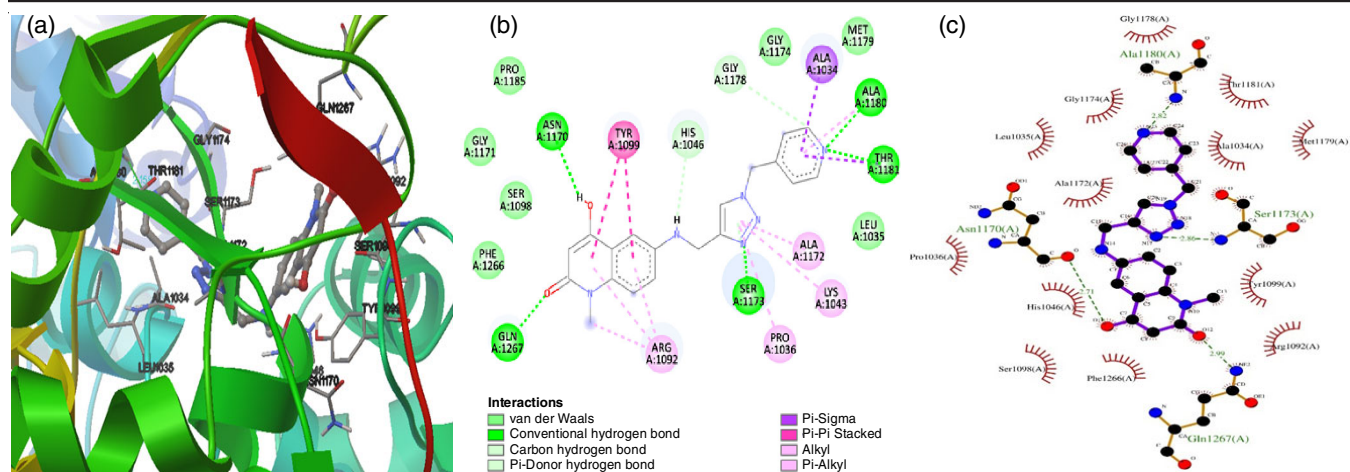
Fig. 1c. (a) 3D-structure, (b) 2D-structure and (c) Ligplot image of ligand **6e**

In this study, we investigated the chemical structural features of compounds (**4a-f** and **6a-f**) in relation to these considerations. The bioavailability radar of complexes and ligands, as depicted in Fig. 2. The consensus log P values for the synthesized compounds range from 0.75-4.01 and all the compounds fulfill the lipophilicity criteria for drug development (Table-4). For all developed compounds, the number of hydrogen bond donors remained constant at two and hydrogen bond acceptors number of hydrogen bond acceptors varied among the compounds, with values of four, seven, eight and ten and the number of bonds that could be rotated, with values of four, five and six. All of the resulting compounds exposed perfect Caco2 permeability with values ranging from –4.71 to –4.97 cm/s.

To investigate BBB membrane permeability, medication distribution, was evaluated and found to be within the range 0.084–0.700 for all drugs, demonstrating that these compounds can cross BBB facilely (Table-4). These findings suggested that all the compounds **4a-f** and **6a-f** have suitable molecular structures that have necessary physico-chemical characteristics and all novel potent units showed high passive permeability in MDCK cell line and Caco-2 models as well as P-glycoprotein [38]. With generally favourable physico-chemical features, all prepared analogues demonstrated effective MACs values that fulfilled the Pfizer rule, the Golden Triangle and the Lipinski

rule to obtain good oral pharmacokinetic outlines [39]. The pink zone of the radar image shows the physico-chemical space required for optimum oral bioavailability (m.w., solubility, insaturation, TPSA, lipophilicity, flexivbility) (Fig. 2). In terms of metabolism, all five common human cytochrome P450 enzymes (CYPs), particularly CYP2C19 and CYP2C9, were predicted to be involved in the metabolism of compounds **4a-f** and **6a-f**. Similar to these compound, they were expected to be the substrates and might be metabolized by mainly CYP2D6 and CYP3A4. Meanwhile, CYP1A2 is the only described enzyme capable of moderately metabolizing triazoles.

The BOILED-Egg model offers an easily reproducible, rapid and statistically unparalleled strategy for predicting both brain permeability and excellent gastrointestinal absorption of small compounds, facilitating their potential use in drug research and discovery [40]. The physico-chemical zone with the highest likelihood of facilitating absorption by the gastrointestinal system is identified in the yolk (the white portion of egg). The Blood-Brain Barrier (depicted in yellow) serves as a chemical and physical barrier preventing substances from entering the brain (BBB penetration). Compounds **4a**, **4b**, **6d** and **6e** showing apparent oral bioavailability, were strategically placed in the BOILED-Egg, as illustrated in Fig. 3. The results indicate that the entire set of synthesized compounds (**4a-f**
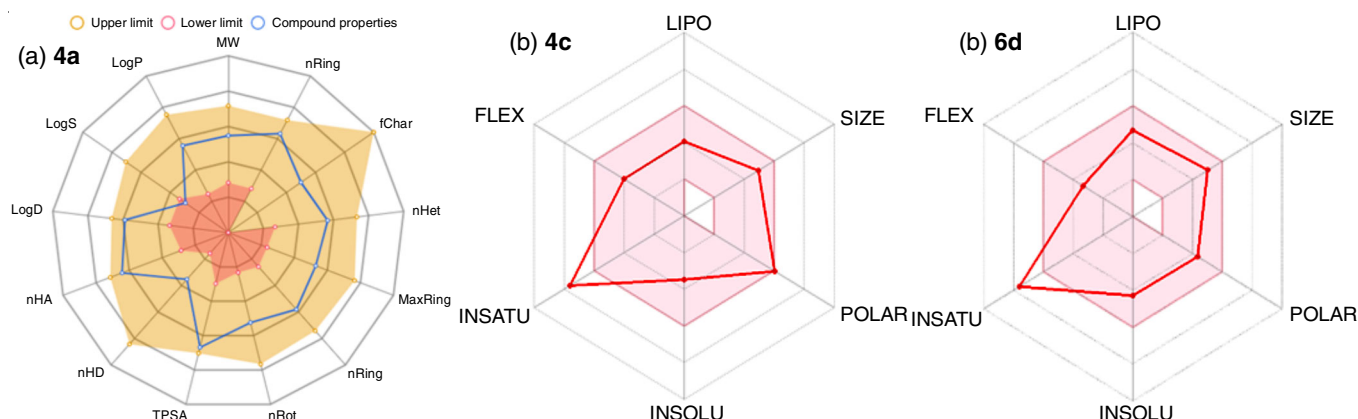

Fig. 2. (a) ADMETlab2.0 platform (**4a**); (b) SwissADME platform (**4c**, **6d**); The pink-coloured zone was identified as the most effective physico-chemical area for oral bioavailability. The figure illustrates lines and dots representing each molecule

TABLE-4
PHYSICO-CHEMICAL, ADMET PROPERTIES AND MEDICINAL CHEMISTRY OF 2-QUINOLONE LINKED TO 1,2,3-TRIAZOLES

	4a	4b	4c	4d	4e	4f	6a	6b	6c	6d	6e	6f
Physico-chemical properties												
nRot	6	5	5	5	5	5	5	4	4	5	4	4
nHBA	10	7	7	7	8	8	10	7	4	7	8	7
nHBD	2	2	2	2	2	2	2	2	2	2	2	2
TPSA	128.11	84.97	84.97	84.97	97.86	97.86	84.96	84.97	84.97	84.97	97.86	84.97
MLogp$_{o/w}$	1.23	3.06	2.57	2.31	1.07	1.07	1.27	2.89	2.62	2.95	1.10	2.35
LogP	1.82	3.17	2.59	1.84	0.77	0.75	2.18	2.06	4.01	3.23	0.77	1.95
LogD	2.54	3.27	3.02	2.275	1.05	1.06	2.55	2.71	3.15	3.34	2.26	2.53
LogS	-4.48	-4.52	-3.49	-3.49	-2.82	-2.72	-5.19	-4.59	-4.80	-5.02	-3.20	-4.44
M.Wt	406.14	429.08	395.11	375.17	362.15	362.15	392.12	383.12	381.82	415.13	348.13	361.15
Absorption												
MDCK score	1.7×10^{-5}	2.2×10^{-5}	1.9×10^{-5}	1.6×10^{-5}	1.2×10^{-5}	1.1×10^{-5}	1.5×10^{-5}	1.6×10^{-5}	1.3×10^{-5}	1.6×10^{-5}	7.9×10^{-6}	1.1×10^{-5}
Caco-2score	-4.97	-4.83	-4.82	-4.91	-4.95	-4.89	-4.81	-4.71	-4.82	-4.76	-4.84	-4.84
Pgp-inhibitor	0.008	0.089	0.024	0.022	0.005	0.004	0.002	0.004	0.008	0.018	0.003	0.007
F(20%)	0.003	0.002	0.004	0.004	0.003	0.003	0.004	0.005	0.002	0.002	0.003	0.003
HIA score	0.007	0.006	0.005	0.006	0.007	0.006	0.006	0.008	0.005	0.004	0.007	0.006
PPB (%)	97.14	98.02	96.91	95.95	93.06	93.74	97.67	97.60	97.90	97.62	94.85	97.01
BBB	0.084	0.140	0.553	0.472	0.700	0.687	0.112	0.134	0.479	0.132	0.536	0.426
Medicinal chemistry												
SA score	2.55	2.56	2.48	2.61	2.55	2.55	2.59	2.52	2.47	2.59	2.61	2.59
Lipinski rule	Yes	Yes	Yes	Yes	Yes	Yes	Yes	Yes	Yes	Yes	Yes	Yes
Pfizer	Yes	Yes	Yes	Yes	Yes	Yes	Yes	Yes	Yes	Yes	Yes	Yes
GSK	No	No	Yes	Yes	Yes	Yes	Yes	Yes	Yes	NO	Yes	Yes
Golden triangle	Yes	No	Yes	Yes	Yes	Yes	Yes	Yes	Yes	Yes	Yes	Yes
Pains	0	0	0	0	0	0	0	0	0	0	0	0
Metabolism												
CYP1A2	0.782	0.948	0.962	0.938	0.968	0.944	0.949	0.952	0.959	0.938	0.961	0.871
CYP2C19	0.753	0.944	0.940	0.937	0.878	0.618	0.507	0.560	0.776	0.800	0.403	0.665
CYP2C9	0.800	0.893	0.872	0.845	0.876	0.720	0.797	0.695	0.597	0.744	0.560	0.598
CYP2D6	0.118	0.584	0.420	0.308	0.173	0.022	0.191	0.322	0.534	0.301	0.265	0.282
CYP3A4	0.795	0.920	0.906	0.863	0.850	0.851	0.819	0.761	0.722	0.741	0.556	0.786
Toxicity												
hERG	0.327	0.256	0.099	0.044	0.390	0.370	0.116	0.167	0.244	0.243	0.354	0.097
H.HT	0.238	0.224	0.248	0.315	0.354	0.324	0.221	0.811	0.242	0.569	0.299	0.301
ROA	0.085	0.074	0.08	0.086	0.075	0.115	0.078	0.270	0.091	0.138	0.247	0.117
AMES	0.961	0.311	0.537	0.583	0.246	0.247	0.952	0.916	0.821	0.880	0.545	0.866
Skin. Sens.	0.448	0.378	0.343	0.148	0.623	0.674	0.375	0.701	0.461	0.194	0.742	0.217
Eyecorr.	0.003	0.003	0.003	0.003	0.003	0.003	0.003	0.003	0.003	0.003	0.003	0.003

HHT: Human hepatotoxicity (1 = possitive, 0 = negative); BBB: blood-brain barrier (0 = log BBB ≤ -1, 1 = log BBB >-1); MDCK: Madin-Darby Canine kidney cells; TPSA: topological polar surface area; Pgp: P-glycoprotein (1 = inhibitor, 0 = non inhibitor); HIA: Human Intestinal Absorbtion (1 = <30%, 0 = ≥ 30%); CYP2C19 inhibitor (1 = inhibitor, 0 = non inhibitor); CYP2C9 inhibitor (1 = inhibitor, 0 = non inhibitor); CYP1A2 inhibitor (1 = inhibitor, 0 = non inhibitor); CYP3A4 inhibitor (1 = inhibitor, 0 = non inhibitor); CYP2D6 inhibitor (0 = non inhibitor); Lipinski rule: < 2 violations. The prediction probability values are converted into six symbols for the classification end points, which are separated into three empirically based decision stages that are visually depicted with totally different colours, including (1) excellent/green: 0-0.1 and 0.1-0.3, (2) medium/yellow: 0.3-0.5 and 0.5-0.7 and (3) red/poor: 0.7-0.9 and 0.9-1.0.
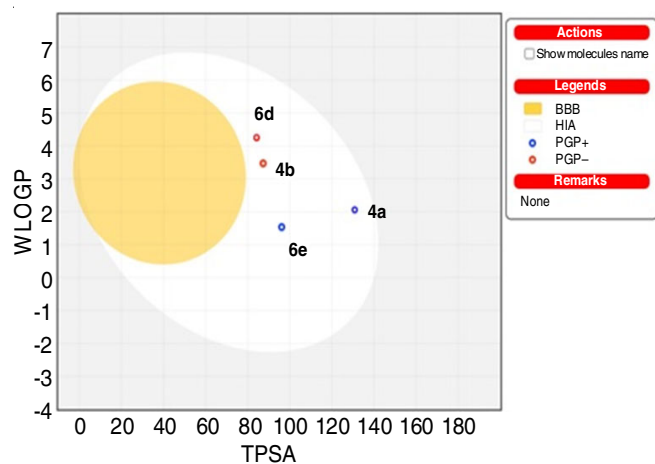
Fig. 3. BOILED-Egg model for predicting final triazoles **4a, 4b, 6d** and **6e**

and **6a-f**) exhibits a range of excellent characteristics associated with high bioavailability. Compounds **4a-f** and **6a-f**, resembling known drugs and subject to investigation, hold promise as potential candidates for further therapeutic development.

Conclusion

In order to discover a new series of 2-quinolone based to 1,2,3-triazoles derivatives were synthesized and their antimicrobial activity was evaluated. Thus, new quinolones conjugated triazole were prepared and characterized by ^{1}H NMR, ^{13}C NMR, mass and IR spectrometric techniques. The results of this study showed that compounds **4a**, **4d**, **6a**, **6b** and **6d** have a promising antimicrobial activity against *S. epidermidis*, *S. aureus*, *P. aeruginosa* bacterial strains and *A. clavatus*, *A. niger* and *C. albicans* (fungal strains). In particular, the scaffolds **4a** and **6d** showed remarkable antibacterial activity against

S. epidermidis, P. aeruginosa strains with MIC values of 6.32 ± 0.04, 2.38 ± 0.01 µg/mL, 3.19 ± 0.04, 8.71 ± 0.01 µg/mL, respectively. Using molecular docking, replications of the active site of DNA gyrase complex protein(2XCO) of *S. aureus*, we studied at how these analogues may interact with the receptor. Meanwhile, the docking results were consistent with biological activities and compounds which demonstrated significant inhibitory activity against antibacterial growth were further examined for their ADMET and physico-chemical characteristics. Thus, the obtained results allow to conclude that these molecules are essential lead compounds for further exploration of the biological activities.

ACKNOWLEDGEMENTS

CONFLICT OF INTEREST

The authors declare that there is no conflict of interests regarding the publication of this article.

REFERENCES

1. A.C. Spencer and S.S. Panda, *Biomedicines*, **11**, 371 (2023);
https://doi.org/10.3390/biomedicines11020371
2. L.A. Mitscher, *Chem. Rev.*, **105**, 559 (2005);
https://doi.org/10.1021/cr030101q
3. T.R. Allaka, B. Kummari, N. Polkam, N. Kuntala, K. Chepuri and J.S. Anireddy, *Mol. Divers.*, **26**, 1581 (2022);
https://doi.org/10.1007/s11030-021-10287-3
4. Z. Dang, Y. Yang, R. Ji and S. Zhang, *Bioorg. Med. Chem. Lett.*, **17**, 4523 (2007);
https://doi.org/10.1016/j.bmcl.2007.05.093
5. F.D.C. da Silva, M.C.B. de Souza, I.I. Frugulhetti, H.C. Castro, S.L.D.O. Souza, T.M.L. de Souza and V.F. Ferreira, *Eur. J. Med. Chem.*, **44**, 373 (2009);
https://doi.org/10.1016/j.ejmech.2008.02.047
6. X. Wang, Z.C. Dai, Y.F. Chen, L.L. Cao, W. Yan, S.K. Li, J.X. Wang, Z.G. Zhang and Y.H. Ye, *Eur. J. Med. Chem.*, **126**, 171 (2017);
https://doi.org/10.1016/j.ejmech.2016.10.006
7. A.S.A.L. Fallah-Tafti, T. Akbarzadeh, P. Saniee, F. Siavoshi, A. Shafiee, and A. Foroumadi, *Turk. J. Chem.*, **35**, 307 (2011);
https://doi.org/10.3906/kim-1004-522
8. S.S. Braga, *Eur. J. Med. Chem.*, **183**, 111660 (2019);
https://doi.org/10.1016/j.ejmech.2019.111660
9. X.M. Chu, C. Wang, W. Liu, L.L. Liang, K.K. Gong, C.Y. Zhao and K.L. Sun, *Eur. J. Med. Chem.*, **161**, 101 (2019);
https://doi.org/10.1016/j.ejmech.2018.10.035
10. N. Razzaghi-Asl, S. Sepehri, A. Ebadi, P. Karami, N. Nejatkhah, and M., Johari-Ahar, *Mol. Divers. 24*, 525, (2020);
https://doi.org/10.1007/s11030-019-09953-4
11. M. Mishra, V.K. Mishra, V. Kashaw, A.K. Iyer and S.K. Kashaw, *Eur. J. Med. Chem.*, **125**, 1300 (2017);
https://doi.org/10.1016/j.ejmech.2016.11.025
12. N. Chokkar, S. Kalra, M. Chauhan and R. Kumar, *Mini Rev. Med. Chem.*, **19**, 510 (2019);
https://doi.org/10.2174/1389557518666181018163448
13. S.R. Patpi, L. Pulipati, P. Yogeeswari, D. Sriram, N. Jain, B. Sridhar, R. Murthy, S.V. Kalivendi and S. Kantevari, *J. Med. Chem.*, **55**, 3911 (2012);
https://doi.org/10.1021/jm300125e
14. M.W. Pertino, C. Theoduloz, E. Butassi, S. Zacchino and G. Schmeda-Hirschmann, *Mol.*, **20**, 8666 (2015);
https://doi.org/10.3390/molecules20058666
15. N.Y. Tashkandi, Z.M. Al-Amshany and N.A. Hassan, *J. Mol. Struct.*, **1269**, 133832 (2022);
https://doi.org/10.1016/j.molstruc.2022.133832
16. A. Rammohan, B.C. Venkatesh, N.M. Basha, G.V. Zyryanov and M. Nageswararao, *Chem. Biol. Drug Des.*, **101**, 1181 (2023);
https://doi.org/10.1111/cbdd.14148
17. R. Raj, P. Singh, P. Singh, J. Gut, P.J. Rosenthal and V. Kumar, *Eur. J. Med. Chem.*, **62**, 590 (2013);
https://doi.org/10.1016/j.ejmech.2013.01.032
18. S. Bitla, S.R. Sagurthi, R. Dhanavath, M.R. Puchakayala, S. Birudaraju, A.A. Gayatri, V.K. Bhukya and K.R. Atcha, *J. Mol. Struct.*, **1220**, 128705 (2020);
https://doi.org/10.1016/j.molstruc.2020.128705
19. J.L. Kelley, C.S. Koble, R.G. Davis, E.W. McLean, F.E. Soroko and B.R. Cooper, *J. Med. Chem.*, **38**, 4131 (1995);
https://doi.org/10.1021/jm00020a030
20. P.E. Lønning, J. Geisler and M. Dowsett, *Breast Cancer Res Treat Title*, **49**, S53 (1998).
21. R. Bollu, J.D. Palem, R. Bantu, V. Guguloth, L. Nagarapu, S. Polepalli and N. Jain, *Eur. J. Med. Chem.*, **89**, 138 (2015);
https://doi.org/10.1016/j.ejmech.2014.10.051
22. D.R. Hou, S. Alam, T.C. Kuan, M. Ramanathan, T.P. Lin and M.S. Hung, *Bioorg. Med. Chem. Lett.*, **19**, 1022 (2009);
https://doi.org/10.1016/j.bmcl.2008.11.029
23. V. Calderone, F.L. Fiamingo, G. Amato, I. Giorgi, O. Livi, A. Martelli and E. Martinotti, *Eur. J. Med. Chem.*, **43**, 2618 (2008);
https://doi.org/10.1016/j.ejmech.2008.02.032
24. V.D. Bock, D. Speijer, H. Hiemstra and J.H. van Maarseveen, *Org. Biomol. Chem.*, **5**, 971 (2007);
https://doi.org/10.1039/B616751A
25. S. Bitla, A.A. Gayatri, M.R. Puchakayala, V.K. Bhukya, J. Vannada, R. Dhanavath, B. Kuthati, D. Kothula, S.R. Sagurthi and K.R. Atcha, *Bioorg. Med. Chem. Lett.*, **41**, 128004 (2021);
https://doi.org/10.1016/j.bmcl.2021.128004
26. K. Saurav and K. Kannabiran, *Rev. Iberoam. Micol.*, **29**, 29 (2012);
https://doi.org/10.1016/j.riam.2011.06.008
27. M. Hu, J. Li, and S.Q. Yao, *Org. Lett.*, **10**, 5529 (2008);
https://doi.org/10.1021/ol802286g
28. H.C. Kolb, M.G. Finn and K.B. Sharpless, *Angew. Chem., Int. Ed. Engl.*, **40**, 2004 (2001);
https://doi.org/10.1002/1521-3773(20010601)40:11<2004::AID-ANIE2004>3.0.CO;2-5
29. F. Sahin, *J. Ethnopharmacol.*, **87**, 61 (2003);
https://doi.org/10.1016/S0378-8741(03)00110-7
30. M. Güllüce, A. Adigüzel, H. Ögütçü, M. Sengül, I. Karaman and F. Sahin, *Phytother. Res.*, **18**, 208 (2004);
https://doi.org/10.1002/ptr.1419
31. ACD/ChemSketch, version 2020.2.1, Advanced Chemistry Development, Inc., Toronto, ON, Canada (2021).
32. S.K. Gandham, A.A. Kudale, T. Rao Allaka and A. Jha, *ChemistrySelect*, **7**, e202200683 (2022);
https://doi.org/10.1002/slct.202200683
33. B.D. Bax, P.F. Chan, D.S.A. Eggleston and D.R. Fosberry, *Nature*, **466**, 935 (2010);
https://doi.org/10.1038/nature09197.
34. G.M. Morris, R. Huey, W. Lindstrom, M.F. Sanner, R.K. Belew, D.S. Goodsell and A.J. Olson, *J. Comput. Chem.*, **30**, 2785 (2009);
https://doi.org/10.1002/jcc.21256
35. G. Gogisetti, U. Kanna, V. Sharma, T. Rao Allaka and B. Rao Tadiboina, *Chem. Biodivers.*, **19**, e202200681 (2022);
https://doi.org/10.1002/cbdv.202200681
36. J.B. Baell and G.A. Holloway, *J. Med. Chem.*, **53**, 2719 (2010);
https://doi.org/10.1021/jm901137j
37. V.R. Gollapalli, H.B. Bollikolla, T.R. Allaka, P.R.R. Vaddi, S. Basireddy, M. Ganivada and S.R. Pindi, *Chem. Biodivers.*, **20**, e202201259 (2023);
https://doi.org/10.1002/cbdv.202201259
38. J.D. Hughes, J. Blagg, D.A. Price, S. Bailey, G.A. DeCrescenzo, R.V. Devraj, E. Ellsworth, Y.M. Fobian, M.E. Gibbs, R.W. Gilles and N. Greene, *Bioorg. Med. Chem. Lett.*, **18**, 4872 (2008);
https://doi.org/10.1016/j.bmcl.2008.07.071
39. A. Daina, O. Michielin and V. Zoete, *Sci. Rep.*, **7**, 42717 (2017);
https://doi.org/10.1038/srep42717
40. B. Bakchi, A.D. Krishna, E. Sreecharan, V.B.J. Ganesh, M. Niharika, S. Maharshi, S.B. Puttagunta, D.K. Sigalapalli, R.R. Bhandare and A.B. Shaik, *J. Mol. Struct.*, **1259**, 132712 (2022);
https://doi.org/10.1016/j.molstruc.2022.132712